ACS APPLIED MATERIALS & INTERFACES

Research Article

www.acsami.org

# Dense Vertically Aligned Copper Nanowire Composites as High Performance Thermal Interface Materials

Michael T. Barako,*[,†,‡] Scott G. Isaacson,[‡] Feifei Lian,[†,‡] Eric Pop,[‡] Reinhold H. Dauskardt,[‡] Kenneth E. Goodson,[‡] and Jesse Tice[†]

[†]NG Next, Northrop Grumman Corporation, One Space Park, Redondo Beach, California 90278, United States

[‡]Stanford University, Stanford, California 94305, United States

Supporting Information

**ABSTRACT:** Thermal interface materials (TIMs) are essential for managing heat in modern electronics, and nanocomposite TIMs can offer critical improvements. Here, we demonstrate thermally conductive, mechanically compliant TIMs based on dense, vertically aligned copper nanowires (CuNWs) embedded into polymer matrices. We evaluate the thermal and mechanical characteristics of 20−25% dense CuNW arrays with and without polydimethylsiloxane infiltration. The thermal resistance achieved is below 5 $mm^2$ K $W^{-1}$, over an order of magnitude lower than commercial heat sink compounds. Nanoindentation reveals that the nonlinear deformation mechanics of this TIM are influenced by both the CuNW morphology and the polymer matrix. We also implement a flip−chip bonding protocol to directly attach CuNW composites to copper surfaces, as required in many thermal architectures. Thus, we demonstrate a rational design strategy for nanocomposite TIMs that simultaneously retain the high thermal conductivity of aligned CuNWs and the mechanical compliance of a polymer.

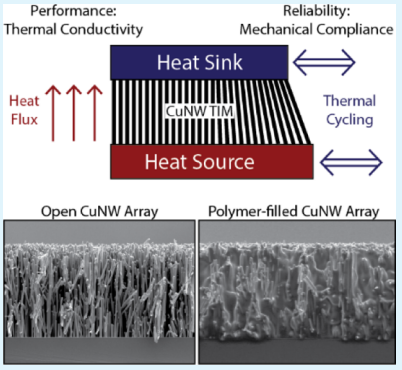


**KEYWORDS:** *TIMs, CuNWs, thermal conductivity, nanoindentation, composites*

## 1. INTRODUCTION

Thermal interface materials (TIMs) provide a low resistance thermal pathway between heat sources and heat sinks by filling the interfacial volume created when two microscopically rough surfaces are in contact.[1−3] An ideal TIM is both thermally conductive, to facilitate heat transfer across the interface, and mechanically compliant to conform to the surface roughness and to maintain the integrity of the interface during thermomechanical stresses imposed by temperature gradients, thermal cycling, and thermal aging. However, these two properties often scale dichotomously, where high thermal conductivity materials are typically dense and stiff, while soft materials are generally thermally insulating. As a result, most commercially available TIMs are either thermally conductive (e.g. solder) or mechanically compliant (e.g. thermal paste) but seldom both. In this work, we demonstrate the use of composites containing dense, vertically aligned copper nanowires (CuNWs) embedded in a soft polydimethylsiloxane (PDMS) matrix to simultaneously achieve both thermal and mechanical requirements of a reliable, high performance TIM.

There are two common strategies used to create thermally conductive and mechanically compliant materials as shown in Figure 1. One approach is to disperse conductive filler particles into a soft material, such as a polymer, to form a percolating conduction network.[4] Composites that contain dispersions of high thermal conductivity nanomaterials (e.g. metal NWs and nanoparticles,[5−8] carbon nanotubes,[8,9] and inorganic nanoparticles[10−12]) can achieve large enhancements in thermal conductivity compared to the unfilled matrix. However, the absolute thermal conductivity of such composites rarely exceeds ∼5 W $m^{-1}$ $K^{-1}$ because of low volume fractions, failure to achieve percolation, contact resistances between particles, and the unaligned orientation of the filler particles.

An alternative approach is to use a conductive bulk material (e.g. metals and graphite) to produce a nanostructured morphology with mechanical compliance. Aligned arrays of continuous, conductive elements define the thermal conductivity limit for porous media by minimizing the effective heat transfer path length and eliminating the need for interparticle conduction (i.e. "continuous" rather than "percolation" network). For over a decade, this approach has focused on synthesizing carbon nanotubes (CNTs) into vertically aligned arrays.[13−16] More recent work has explored the use of templated electrodeposition to grow vertically aligned metal NWs,[1,17−19] which circumvent many of the challenges facing CNTs including harsh growth conditions, limited capability to tune morphology, and the wide disparity in reported thermal conductivities because of variations in network morphology.[13,20−22] Here, we establish vertically aligned CuNW arrays with insertable polymer matrices as high performance TIMs, we characterize their combined

Received: August 16, 2017
Accepted: November 9, 2017
Published: November 9, 2017





DOI: 10.1021/acsami.7b12313
ACS Appl. Mater. Interfaces 2017, 9, 42067−42074

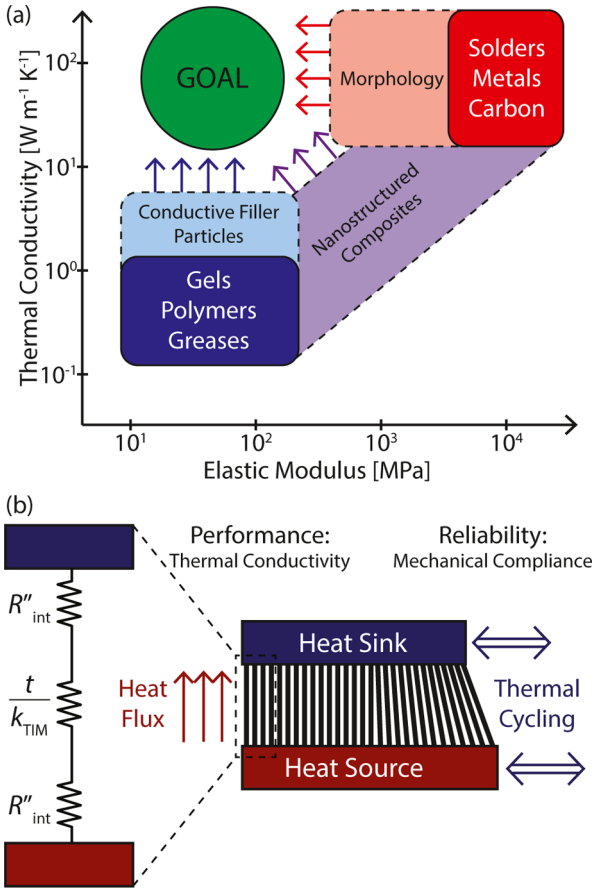


**Figure 1.** (a) Two common strategies are employed to create composites with high thermal conductivity and mechanical flexibility. One strategy is to begin with an intrinsically soft material and add fillers to increase the thermal conductivity. The second strategy is to nanostructure an intrinsically conductive material into a mechanically compliant morphology. Nanostructured composites result from the blending of both strategies. (b) Composite thermal interface materials have a total thermal resistance derived from three serial resistances: the hot-side interface, the volumetric conduction resistance, and the cold-side interface. As the intrinsic thermal conductivity of the TIM $k_{TIM}$ increases, the contribution of the two interface resistances become dominant.

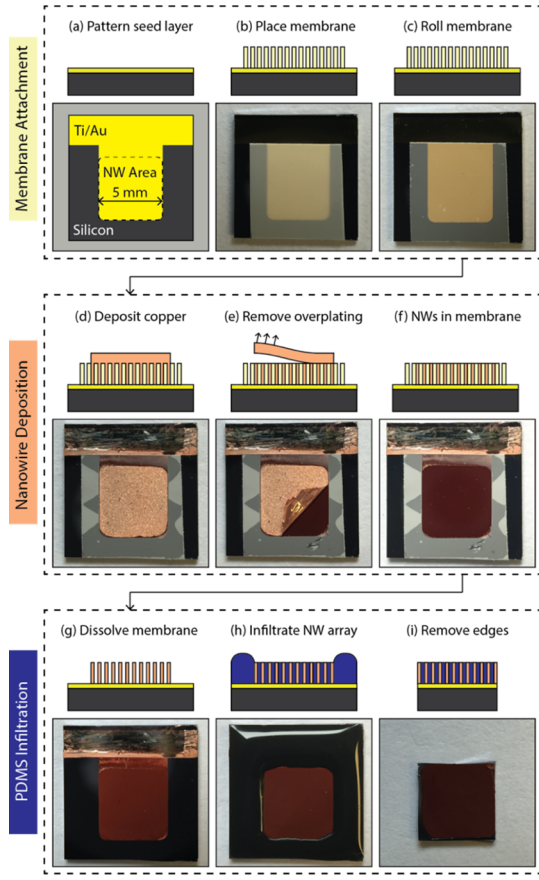


**Figure 2.** Schematics and photographs showing the synthesis of composites containing vertically aligned CuNWs embedded in PDMS. (a) A seed layer is patterned onto the substrate, and (b) a polycarbonate membrane is placed on the substrate and (c) rolled smooth. (d) Copper is electrodeposited through the membrane pores (the NWs) and over the top of the membrane (the overplating). (e) The overplating is peeled away to (f) reveal the NW array. (g) The membrane is dissolved to liberate the NWs. (h) A polymer is placed around the perimeter, where it infiltrates the array via capillary wicking. (i) After cross-linking the polymer, the excess material is removed.

thermal and mechanical property data, and we demonstrate practical device integration.

We use vertically aligned arrays of CuNWs to provide a mechanically compliant and high thermal conductivity material architecture, as shown in Figure 2. This morphology provides continuous, parallel thermal conduits where heat is not required to conduct across NW−NW contacts, such as those found in percolation networks. In addition, the vertical alignment provides the shortest conduction path across an interface that can approach the theoretical rule-of-mixture limit for parallel conductors.[23] Electrodeposited CuNW arrays have been shown to possess intrinsic thermal conductivities as high as 70 W $m^{-1}$ $K^{-1}$ at densities approaching 25%.[17] These arrays can be synthesized over large areas (~$cm^2$, see Supporting Information section S1), exhibit high degrees of alignment and uniformity and have tunable properties that preserve the high conductivity of the constituent NWs.

However, there are two critical requirements imposed on CuNW arrays for practical device integration as a TIM: the need to exhibit desirable mechanical properties such as toughness and elasticity, and the need to attach the array to the adjacent surfaces for both interface integrity and minimal contact resistance. While freestanding CuNWs are flexible and compliant, the arrays experience plastic deformation under mechanical loading that causes poor contact to the adjacent surface and irreversible structural changes to the morphology. We mitigate this challenge by infiltrating the CuNW array with a polymer matrix. This matrix preserves the array morphology, provides an elastic mechanical response to loading, protects the NWs from oxidation and other environmental damage, and permits the array to be handled and processed without degrading the thermal conductivity. This strategy decouples the thermal and mechanical properties of the composite by selecting high-contrast constituent phases that each achieve one of the two requirements. Thermal conduction occurs primarily in the aligned CuNWs, and the polymer matrix imbues the array with improved mechanical properties. Each phase provides distinct and desirable properties to the overall composite. The conduction pathway is continuous along the length of the NWs such that heat is not forced to conduct through the insulating polymer matrix, and the high aspect ratio


DOI: 10.1021/acsami.7b12313
ACS Appl. Mater. Interfaces 2017, 9, 42067−42074

of the NWs allows the array to flex and deform with the elastomeric matrix.

## 2. EXPERIMENTAL SECTION

**2.1. Synthesis of Vertically Aligned CuNW Composites.** We synthesize the CuNW composites using a combination of templated electrodeposition (to form the NW array) and capillary infiltration (to embed the NWs in a polymer matrix). The freestanding CuNW arrays are synthesized using a derivative of the protocol in ref 17 as shown in Figure 2. A thin metal seed layer (5/50 nm of Ti/Au) is deposited through a shadow mask onto a silicon substrate using electron beam evaporation (Figure 2a), and a porous polycarbonate track-etched membrane (Sterlitech Inc.) is electrostatically adhered to the surface (Figure 2b,c). We use three different membranes having different pore sizes and porosities to produce NWs with diameters of 320, 470, and 1190 nm and volume fractions between 20 and 25% (see Table 1).

**Table 1. Vertically Aligned CuNW Array configurations**[17]

| nominal pore diameter [nm] | measured CuNW diameter [nm] | array thickness [$\mu$m] | aspect ratio | uncompressed volume fraction [%] |
|---|---|---|---|---|
| 200 | 322 ± 6 | 31.6 ± 0.1 | 98 ± 2 | 19.5 ± 1.6 |
| 400 | 466 ± 38 | 27.4 ± 0.2 | 59 ± 5 | 22.2 ± 5.7 |
| 1000 | 1189 ± 45 | 28.7 ± 0.2 | 24 ± 1 | 23.3 ± 3.0 |

Potentiostatic electrodeposition (Figures 2d and S1) is used to deposit copper onto the seed layer, up through the pores, and over the top of the membrane from an aqueous electrolyte of 0.6 M $CuSO_4$ and 30 mM $H_2SO_4$ (pH = 1.7). The NWs are grown using a three-electrode electrochemical cell[17] at an applied voltage of −320 mV versus Ag/AgCl for 30 min to fill the pores, followed by an additional 15 min at −400 mV versus Ag/AgCl to thicken the sacrificial overplating. Sharp tweezers are used to lift the corner of the overplating and peel it away from the top surface of the membrane (Figure 2e,f). The polycarbonate membrane is dissolved in dichloromethane at 50 °C to produce a freestanding array (Figure 2g).

A low viscosity two-part PDMS (Sylgard 170, Dow Corning Inc., viscosity $\upsilon$ = 2300 cP, thermal conductivity $k_{PDMS}$ = 0.4 W m$^{-1}$ K$^{-1}$) is mixed at a 1:1 volume ratio and placed along the perimeter of the array (Figure 2h). The polymer slowly wicks into the interstitial volume between the NWs, which takes approximately 1 h for the arrays presented here (5 mm × 5 mm). The infiltration front is observed by the change in color from a light brown to a dark brown in the wetted areas. The use of lateral infiltration from an external reservoir and capillary-driven flow provides a self-regulating level of filling, which allows the polymer to fill the interstitial volume of the array up to the NW tips without excess. The PDMS cures over 24 h under ambient conditions, and the excess material around the perimeter of the array is cut away. The final CuNW/PDMS composite is ∼30 $\mu$m thick and covers the entire surface of a 5 mm × 5 mm silicon chip (Figure 2i). This technique takes advantage of the intrinsic scalability and simplicity of both electrodeposition and templated nanostructuring. CuNW arrays grown using this method can be scaled up to arbitrarily large dimensions, only limited by the size of the membrane template.

**2.2. Thermal Property Measurements.** We measure the thermal properties of the CuNW composites using an implementation of the ASTM D5470 testing protocol (see Methods, Supporting Information section S2).[1,15,24] The total thermal resistance is measured using one-dimensional steady state measurement apparatus with pressure control (see Figure S2). The sample is compressed between two copper metering bars to a prescribed load (from ∼1 to 5 MPa measured using an in-line load cell). A PID-controlled heat source at the top of the metering bar and a heat sink at the bottom of the other metering bar generate one-dimensional heat flow along the metering bars and through the sample. The temperature is recorded at four locations along each metering bar, and the heat flux is calculated using Fourier's law. For the measurements in this study, we use a temperature of 50 °C to establish a temperature gradient above ambient (∼25 °C). The two reference bars provide bounds on the heat flux conducting across the sample; the bar adjacent to the heat source measures the heat flow into the sample, whereas the bar adjacent to the heat sink measures the heat flow out of the sample. The difference in measured heat flow corresponds to the heat dissipated to the ambient over the length of the apparatus. The temperature across the sample is calculated by extrapolating the linear regression temperature profile in each metering bar to the location of the sample (see Supporting Information, eq S3). The total thermal resistance of the sample $R''_{measured}$ is calculated by dividing the temperature difference across the sample by the heat flux. Because the samples are on silicon substrates (and beneath copper substrates for the bonded samples), we isolate the total resistance of the CuNW/PDMS composites ($R''_{TIM,total}$ = $R''_{int,growth}$ + $R''_{CuNW/PDMS}$ + $R''_{int,tip}$, see eq 2) by subtracting any additional resistances in the sample stack (see Supporting Information section S2).

**2.3. Mechanical Property Measurements.** The mechanical properties of the CuNW composites are characterized using an iNano nanoindenter (Nanomechanics, Inc., Oak Ridge, TN) equipped with a 50 $\mu$m diameter diamond flat punch tip. The nanoindentation measurements are performed using a continuous stiffness measurement (CSM) technique. Sixteen independent indentations are made on each sample, with individual indentations spaced at least 100 $\mu$m apart. Each indentation is performed with a constant target indentation

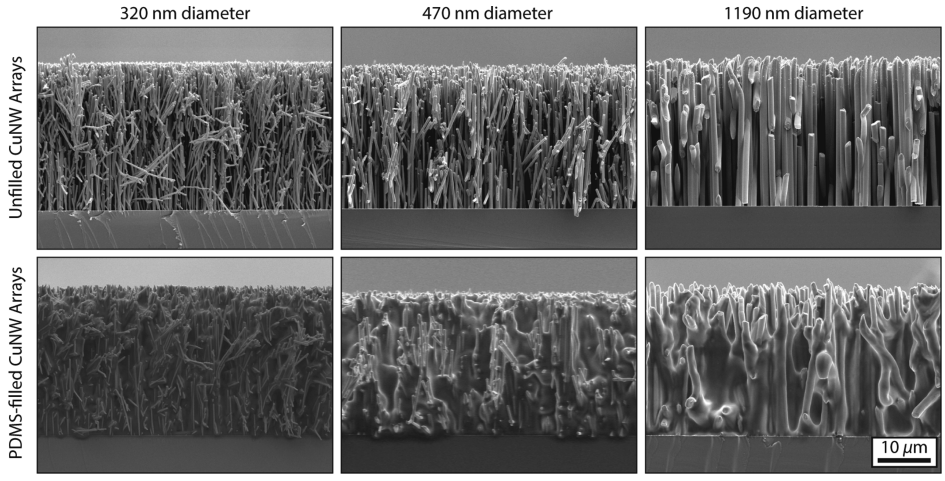


**Figure 3.** Scanning electron microscopy images of vertically aligned CuNW arrays, including (top row) unfilled arrays and (bottom row) composite arrays infiltrated with PDMS. All images are at the same scale.


DOI: 10.1021/acsami.7b12313
ACS Appl. Mater. Interfaces 2017, 9, 42067−42074

strain rate of 0.2% $s^{-1}$, a target CSM frequency of 100 Hz, and a target dynamic displacement of 2 nm. Before each indentation, the drift in displacement is monitored and the measurement is delayed until a drift of less than 0.1 nm/s is achieved. No post-test drift corrections are applied to the data.

## 3. RESULTS AND DISCUSSION

The as-fabricated CuNWs are well-aligned because of the physical template, but it is critical to ensure that viscous flow during infiltration with an interstitial matrix does not disrupt the morphology. We selected a low viscosity PDMS for capillary infiltration to minimize the forces exerted on the NWs. Alternatively, a more viscous polymer can be diluted with a low viscosity and volatile solvent, such as hexane, to promote infiltration. We use cross-sectional scanning electron microscopy (SEM) to verify that the infiltration process does not collapse the NWs (see Figure 3). Furthermore, we demonstrate that the PDMS matrix preserves the array morphology during compression of the composites up to stresses of ~5 MPa (see Supporting Information section S2). The PDMS matrix additionally serves an important role in protecting the CuNWs from oxidation. Using transmission electron microscopy, we have observed a ~10 nm shell of oxidized copper on unprotected NWs that have been exposed to ambient conditions for several days. The use of a polymer matrix is expected to reduce the exposure of metallic copper to ambient oxygen, contaminants, or other reactive species. We have observed no appreciable changes in thermal resistance for CuNW/PDMS composites that have been stored under ambient conditions for as long as one month. However, more aggressive and/or accelerated lifetime testing is required to confirm the long-term stability under realistic operating conditions.

We establish a baseline for the total TIM thermal resistance per unit area $R''_{TIM,total}$ using spin-cast PDMS on silicon without any CuNWs. For PDMS films of comparable thickness to the CuNW arrays, $R''_{TIM,total}$ exceeds ~100 mm$^2$ K W$^{-1}$ or is nearly 2 orders of magnitude larger than that of the CuNW/PDMS composites. By contrast, the CuNW/PDMS composites exhibit pressure-dependent $R''_{TIM,total}$ as low as 1−5 mm$^2$ K W$^{-1}$. These composites outperform many CNT-based TIMs[1,15,16] found in the literature and are comparable to the highest performing nanostructured TIMs (copper nanosprings bonded with indium[1] with $R''_{TIM,total}$ of 0.9 ± 0.4 mm$^2$ K W$^{-1}$).

We measured eight CuNW/PDMS composites to demonstrate repeatability and consistency and to examine the effect of the NW aspect ratio on TIM performance. The thermal measurement data are presented in Figure 4, and the total measured resistance $R''_{measured}$ of all eight samples exhibits consistency and collapses into a narrow band onto a single curve within the measurement uncertainty (see Supporting Information section S2). CuNW/PDMS composites have an intrinsic thermal conductivity $k_{CuNW/PDMS}$ = 40−70 W m$^{-1}$ K$^{-1}$ or equivalently an intrinsic thermal resistance $R''_{CuNW/PDMS}$ = 0.4−0.8 mm$^2$ K W$^{-1}$ for 30 $\mu$m-thick films.[17] This suggests that the thermal interface resistances are the dominant contribution to the total thermal resistance. The exact contribution of the individual interfaces depends on the morphology of the interface, which is inherently coupled to the compressive loading and is difficult to isolate and independently measure. We instead estimate the interface effects using a differential analysis, where the difference in the measured resistance $R''_{TIM,total}$ and $R''_{CuNW/PDMS}$ corresponds to the contributions from

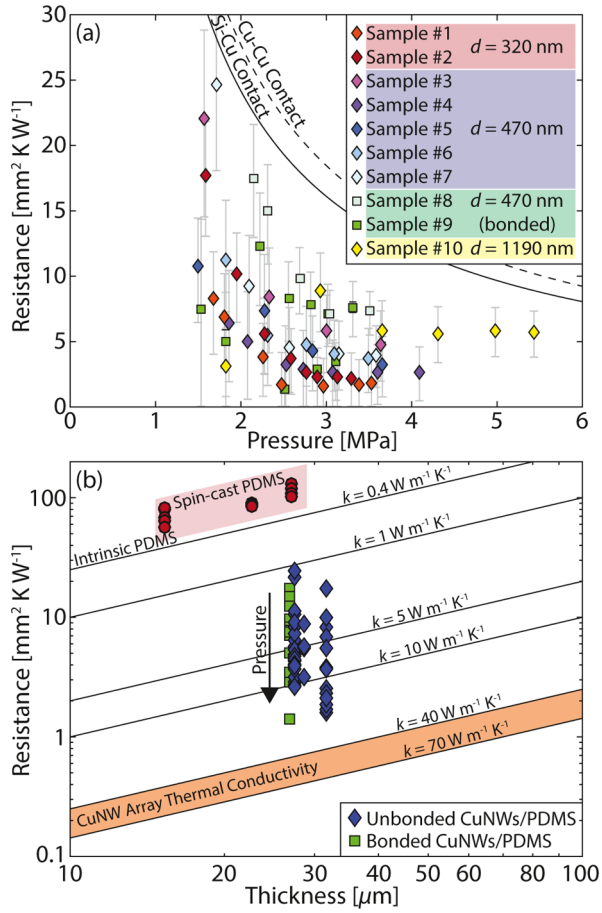


**Figure 4.** (a) Measured thermal resistance as a function of applied pressure for CuNW/PDMS composite TIMs. (b) Thermal resistance plotted vs uncompressed film thickness. These composite TIMs can approach ~1 mm$^2$ K W$^{-1}$ under compression. The strong pressure-dependence (see the downward arrow) is indicative of contact resistance at the composite surface.

the interfaces. Because $R''_{CuNW/PDMS}$ is approximately an order of magnitude less than $R''_{TIM,total}$, we hypothesize that the combined interface resistance is primarily attributed to the contact resistance at the NW tips $R''_{int,tip}$ with minor contributions from the growth interface at the base of the NWs $R''_{int,growth}$ and changes in the composite morphology under compression (which changes the intrinsic thermal conductivity of the composite).

By holding the uncompressed volume fractions approximately constant across the different arrays at 18−25%, we minimize the variation in intrinsic array thermal conductivity. The NWs used in the present work each have diameters much larger than the mean free path of the heat-carrying electrons, and each of the NWs exhibits diffusive-like thermal conduction that is independent of its size. There is a minor trend observed in Figure 4a which suggests that increasing the NW aspect ratio decreases the total thermal resistance, particularly at higher pressures. Because of the small contribution of intrinsic thermal resistance, this variation is likely attributed to the density of interfacial contact points and the mechanical compliance of those contact points. A more flexible NW will more readily conform to adjacent surface roughness and reduce the contact resistance,[14] which is one of the key advantages to using vertically aligned nanostructures for TIMs. However, these effects are smaller than the measurement uncertainty, and


DOI: 10.1021/acsami.7b12313
ACS Appl. Mater. Interfaces 2017, 9, 42067−42074

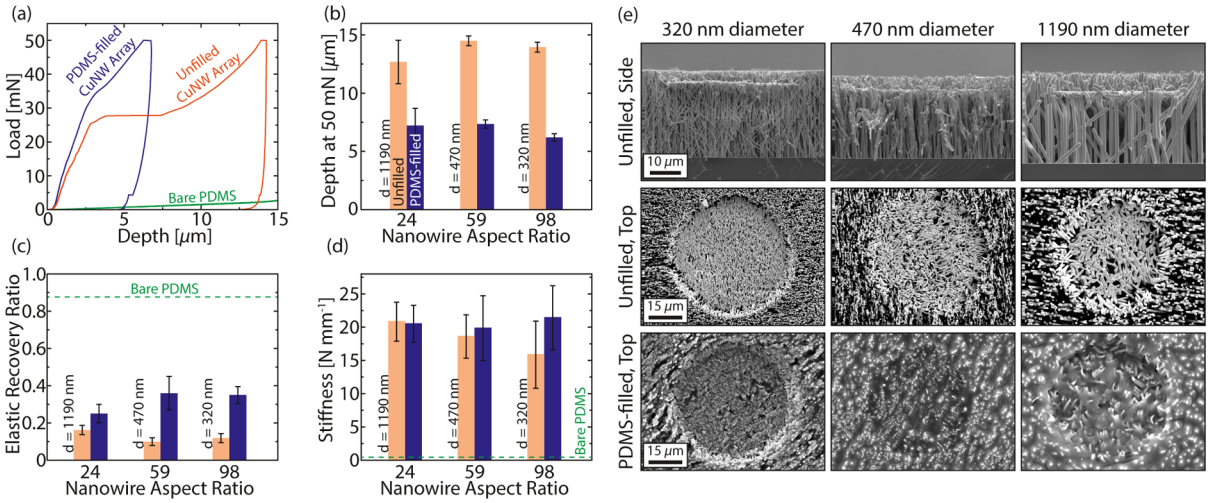


**Figure 5.** Mechanical characteristics of vertically aligned CuNW arrays (~30 μm thick) and spin-cast PDMS films (23 μm thick) subjected to nanoindentation. (a) Representative load–depth curves for an unfilled and a PDMS-filled CuNW array (320 nm NW diameter) and a spin-cast PDMS film. (b) The contact depth at a 50 mN nanoindentation load was significantly higher for unfilled arrays than for PDMS-filled arrays. (c) PDMS-filled arrays exhibited a higher elastic recovery ratio than unfilled arrays. Spin-cast PDMS films exhibited significantly higher recovery ratios and (d) lower stiffnesses than both unfilled and PDMS-filled arrays. (e) Scanning electron micrographs taken after nanoindentation at ~5 μm of compressive displacement to show the deformation morphology of the unfilled and PDMS-filled arrays. All error bars mark one standard deviation from the mean.

instead, the effects of the NW diameter and density primarily manifest in the mechanical properties of the array.

In addition to the thermal properties, we characterize the deformation mechanics of both unfilled and PDMS-filled CuNW arrays. Any nanostructured TIM necessarily experiences both mechanical loading during packaging and thermomechanical stresses during operation. In particular, the CuNW array must be capable of sustaining deformation and compression to prevent failure at the interface. NW fracture events or TIM delamination can lead to an instantaneous increase in thermal resistance and can cause catastrophic device failure. By design, vertically aligned CuNW arrays are highly anisotropic materials, which render their deformation mechanics during compressive loading both complex and important to understand.

The mechanical characteristics of nanostructured TIMs are typically measured using nanoindentation, and such mechanical properties have been measured for arrays of vertically aligned CNTs[14,25−31] and metal oxide NWs[32] as well as individual metal NWs.[33−38] While the CuNWs in the present work exhibit much better alignment than CNT arrays, deviations from the nominal morphology and interactions between adjacent NWs have a pronounced impact on the array-scale mechanical response compared to the properties of an individual NW. Relatively few studies have characterized the mechanical behavior of metallic NW arrays.[39] Although the array thermal conductivity is comparatively invariant with the NW diameter (for CuNWs, with diameters >100 nm and operating near room temperature), the mechanical properties of the array depend much more strongly on the aspect ratio of the constituent NWs and the complex interactions between neighboring NWs.

We characterize the mechanical properties using nanoindentation, where indentations are made on unfilled CuNW arrays, PDMS-filled CuNW composites, and spin-cast PDMS films. Representative load–depth curves are shown in Figure 5a, and the full set of nanoindentation load–depth curves is shown in Supporting Information Figure S8. The unfilled arrays exhibit a characteristic plateau in their load–depth curves beginning at a contact depth of approximately 3 μm (~10% compressive strain) that corresponds to a sharp peak in the time derivative of the indentation depth. This behavior suggests a rapid collapse of the NWs in the array through simultaneous buckling and deformation that leads to an increase in indentation depth at constant load. A similar behavior has also been observed during the nanoindentation of arrays of metal oxide NWs.[32] It should be noted that the relatively small amount of elastic recovery after indentation demonstrates that the rapid collapse of unfilled arrays is not due to purely elastic buckling, but rather a combination of both buckling and plastic deformation. This complex behavior is likely due to frictional interactions between individual NWs in the unfilled arrays. The SEM images (Figure 5e) show that most NWs appear to be in contact with at least one neighboring NW, thus constraining the buckling of individual CuNWs and coupling their deformation to adjacent NWs. The buckling behavior observed in unfilled arrays demonstrates that such materials are vulnerable to sudden deformation that could lead to delamination and catastrophic failure of unfilled CuNW arrays as TIMs.

With a few discrete exceptions, PDMS-filled CuNW arrays exhibit no such buckling plateaus and thus are protected against sudden collapse. The lack of rapid collapse in PDMS-filled CuNW arrays under compressive loading is likely due to the constraining influence of the PDMS between the individual CuNWs, which restricts the lateral displacements necessary for buckling to occur. The elimination of buckling deformation also leads to an overall reduction in the deformation of the NW array under load. Figure 5a shows representative load–depth curves for a PDMS-filled array, an unfilled array, and a spin-cast PDMS film. Both PDMS-filled and unfilled arrays are significantly stiffer than PDMS films because of the high loading fraction of copper. Furthermore, PDMS-filled arrays exhibit less compressive strain at a given load than unfilled arrays. Figure 5b shows that the indentation depth resulting from a 50 mN load on a 50 μm diameter flat punch (~25 MPa) is approximately two times larger for unfilled arrays than for


DOI: 10.1021/acsami.7b12313
ACS Appl. Mater. Interfaces 2017, 9, 42067−42074

PDMS-filled arrays and is only weakly dependent on NW diameter.

Both unfilled and PDMS-filled arrays exhibit partial elastic recovery upon unloading. By contrast, spin-cast PDMS films show nearly complete elastic recovery, even after indentation to a depth of 15 $\mu$m. The degree of elastic recovery after nanoindentation is quantified by the recovery ratio, RR

$$\mathrm{RR} = 1 - \frac{h_f}{h_{max}} \quad (1)$$

where $h_f$ is the indentation depth at zero load upon unloading and $h_{max}$ is the maximum contact depth for a particular indentation (see Supporting Information section S3). The PDMS-filled arrays consistently exhibit a higher degree of elastic recovery than the unfilled NW arrays (Figure 5c). The increased recovery in PDMS-filled composites demonstrates that an elastomeric matrix can mitigate unwanted plastic deformation in CuNW-based TIMs that may occur during bonding or operation.

We also characterize the initial compressive stiffness of the CuNW arrays and spin-cast PDMS films. For the unfilled and PDMS-filled arrays, the stiffness is measured by averaging the slopes of the load−depth curves between nanoindentation loads of 5 and 10 mN. The stiffness of PDMS films is characterized between nanoindentation loads of 0.1 and 1.0 mN. Figure 5d shows that all of the arrays are over an order of magnitude stiffer than spin-cast PDMS films. Neither PDMS infiltration nor the NW aspect ratio has a strong influence on the NW array stiffness. Initial measurements suggest that PDMS infiltration may increase the NW array stiffness slightly over unfilled NW arrays at higher NW aspect ratios, but additional studies are required to confirm the statistical significance of this observation.

There is a complex interplay between the thermal properties and the deformation mechanics as linked by the array morphology and microstructure. The diameter (and aspect ratio) of the individual NWs has a negligible effect on the intrinsic thermal conductivity[17] but a pronounced effect on the mechanics of the NWs. Under compression, the contact surface of the NWs tends to flatten and locally densify, whereas the underlying alignment and density tends to remain undisturbed (see Figure 5e), even at extreme compressive strain rates up to ~50%. The intrinsic thermal conductivity, which generally increases with the volume fraction for a particular morphology, remains approximately constant during compression. However, the intrinsic TIM resistance $R''_{TIM}$ will decrease because of the reduced bondline thickness during compression. The interfacial contact resistance $R''_{int,tip}$ decreases with the areal density and therefore decreases during compression because of a combination of these morphological changes and the additional contact force between surfaces. As the NWs bend and deform, interface morphology changes from point contacts to line contacts as the NWs fold over and agglomerate. Such deformation mechanics have been described in the literature for CNT arrays,[14] which are morphologically similar to NW arrays. By contrast, the growth interface resistance $R''_{int,growth}$ is expected to remain unchanged under compression because the array remains attached to the substrate, and no appreciable deformation is observed to propagate to the base of the NWs.

The requirement of device integration is a common bottleneck to practical implementation of many nanostructured TIMs. As the thermal conductivity of the TIM increases, the interfaces between the TIM and the adjacent surfaces become the dominant resistance to heat transfer. The total thermal resistance (per unit area) $R''_{TIM,total}$ of any nanostructured TIM is the summation of three serial resistances per unit area as shown in Figure 1b

$$R''_{TIM,total} = R''_{int,1} + R''_{TIM} + R''_{int,2} \quad (2)$$

where $R''_{TIM}$ is the intrinsic resistance of the TIM ($R''_{TIM} = t/k_{TIM}$, where $t$ is the thickness and $k_{TIM}$ is the intrinsic thermal conductivity) and $R''_{int}$ is the contact resistance between the TIM and each adjacent surface. We minimize one interface resistance $R''_{int}$ by synthesizing the CuNWs directly on one of the surfaces (the "growth" surface, $R''_{int,growth}$).[17] This provides a chemical bond between the base of each NW and the growth substrate. However, the other interface requires a bonding procedure to attach the free ends of the CuNWs to the adjacent surface. We develop a thermally conductive metallic bond[40] between the CuNW composite and the adjacent surface (here a piece of solid copper) to minimize $R''_{int,tip}$ and improve mechanical attachment.

The CuNW/PDMS composites are thus attached to copper surfaces using an industry standard flip−chip bonding procedure (see Figure 6), which is a common process in

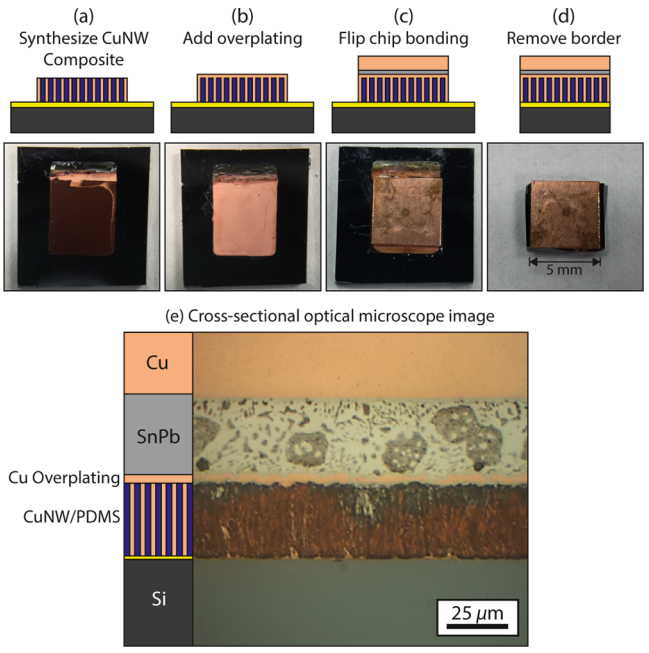


**Figure 6.** (a−d) Schematics and photographs of the process used to bond CuNW composites to copper surfaces. (e) Cross-sectional optical microscopy shows the different layers between the copper and silicon substrate.

microelectronics packaging. Many nanostructured TIMs exhibit large contact resistances to the adjacent surfaces, which becomes the principal bottleneck to heat flow when the thermal conductivity of the TIM is improved. Thin, metallic bonding layers reduce the parasitic resistance at this interface and demonstrate the practical implementation of CuNW/PDMS composite TIMs between heat-generating semiconductor chips and metallic thermal management components (e.g. heat spreaders and heat pipes). There are two methods to form a continuous solid surface for bonding over the tips of the CuNWs. In this work, we synthesize the array as shown in


DOI: 10.1021/acsami.7b12313
ACS Appl. Mater. Interfaces 2017, 9, 42067−42074

Figure 2 and subsequently electroplate an additional ∼5 μm copper film on top of the composite. An alternative method uses the original overplating from the growth process (Figure 2d) as the bonding surface. In this case, the growth protocol is modified such that the bonding process is inserted after Figure 2d, and the remainder of the growth protocol is restarted at Figure 2f. However, while this eliminates the need to deposit additional layers, the now-bonded stack must be exposed to all subsequent processing steps (membrane dissolution and PDMS infiltration), which may limit the utility of the process in many applications.

The target substrate (to which the CuNW composite is to be bonded) is prepared by electroplating the $Sn_{60}Pb_{40}$ solder onto one side of a copper chip, which is chosen as a representative surface to demonstrate the utility of CuNW TIMs for copper heat spreaders and other thermal management components. Solder flux is painted on the solder surface, which is then aligned and compressed at 200 kPa against the CuNW/PDMS composite using a flip−chip bonder. The pressure is then released and the stack is heated at 200 °C for <30 s to reflow the solder and form a bonded Si−(CuNW/PDMS)−Cu interface.

Furthermore, bonded CuNW/PDMS composites have comparable resistivities to the unbonded composites (see Figure 4) while providing the advantage of mechanical attachment between the two surfaces. The bonding layer used in the present work is used as a proof-of-concept to demonstrate the capability to use metallic bonding to anchor these composites to adjacent substrates. However, the end application requirements will drive the optimization of the bonding layer and processing conditions. While bonding nominally reduces the contact resistance, the resistance of the SnPb bonding layer itself adds to the total TIM resistance. This effect can be minimized by optimizing the bonding layer composition and thickness to provide interfacial integrity but limit the introduction of additional resistance.

## 4. CONCLUSIONS

In conclusion, this work demonstrates both the composite design strategy and the high thermal conductivity of CuNW arrays incorporated into elastomeric matrices. These composites are mechanically compliant with thermal resistance below 5 $mm^2\ K\ W^{-1}$. This result is over an order of magnitude better than commercially available heat sink compounds. Furthermore, we demonstrate a realistic device configuration by bonding the TIM between silicon and copper. The techniques presented here are intrinsically inexpensive, scalable, and require only benchtop equipment and ambient conditions. The thermal properties of these composites can be further improved by increasing both the density and alignment of the NWs in the array. While some applications are amenable to direct on-substrate CuNW growth, many applications require an insertable and/or reworkable TIM. To improve the utility and applicability of CuNW-based TIMs, the technological maturation of these composites should move toward the development of freestanding form factors, either as a dry film or a tape (with adhesive surfaces) using the same arrangement of vertically aligned CuNWs embedded in a polymer. Furthermore, additional testing is required to provide application-oriented reliability metrics (e.g. thermal cycling, thermal aging, and vibration), which are essential for demonstrating the long-term durability and reworkability required in nearly all thermal interface applications. These critical factors required for practical application, ranging from manufacturability and form factor to reliability and reworkability, are areas of ongoing research.

## ■ ASSOCIATED CONTENT

### Supporting Information

The Supporting Information is available free of charge on the ACS Publications website at DOI: 10.1021/acsami.7b12313.

Additional details of the material synthesis, thermal metrology, and mechanical measurements (PDF)

## ■ AUTHOR INFORMATION


### Corresponding Author

*E-mail: mbarako@alumni.stanford.edu.

### ORCID

Michael T. Barako: 0000-0002-4745-4515

Eric Pop: 0000-0003-0436-8534

Reinhold H. Dauskardt: 0000-0003-3989-362X


### Notes

The authors declare no competing financial interest.

## ■ ACKNOWLEDGMENTS

The authors would like to thank Conor Coyan for assisting with the polymer infiltration, Allison Yau for assisting with transmission electron microscopy, Tim Akins for assisting with nanowire growth, and Teresa Ha and Gershon Akerling for implementing the flip−chip bonding protocol. This work was supported in part by the National Science Foundation Engineering Research Center for Power Optimization of Electro Thermal Systems (POETS) with cooperative agreement EEC-1449548.

## ■ REFERENCES


(1) Bar-Cohen, A.; Matin, K.; Narumanchi, S. Nanothermal Interface Materials: Technology Review and Recent Results. *J. Electron. Packag.* **2015**, *137*, 040803.

(2) Prasher, R. Thermal Interface Materials: Historical Perspectives, Status, and Future Directions. *Proc. IEEE* **2006**, *94*, 1571−1586.

(3) Sarvar, F.; Whalley, D. C.; Conway, P. P. *Thermal Interface Materials—A Review of the State of the Art. In Electronics System Integration Technology Conference*; Dresden: Germany, 2006; pp 1292−1302.

(4) Idumah, C. I.; Hassan, A. Recently Emerging Trends in Thermal Conductivity of Polymer Nanocomposites. *Rev. Chem. Eng.* **2016**, *32*, 413−457.

(5) Balachander, N.; Seshadri, I.; Mehta, R. J.; Schadler, L. S.; Borca-Tasciuc, T.; Keblinski, P.; Ramanath, G. Nanowire-Filled Polymer Composites with Ultrahigh Thermal Conductivity. *Appl. Phys. Lett.* **2013**, *102*, 093117.

(6) Munari, A.; Xu, J.; Dalton, E.; Mathewson, A.; Razeeb, K. M. Metal Nanowire-Polymer Nanocomposite as Thermal Interface Material. *59th IEEE Electronic Components and Technology Conference*, 2009; pp 448−452.

(7) Wang, S.; Cheng, Y.; Wang, R.; Sun, J.; Gao, L. Highly Thermal Conductive Copper Nanowire Composites with Ultralow Loading: Toward Applications as Thermal Interface Materials. *ACS Appl. Mater. Interfaces* **2014**, *6*, 6481−6486.

(8) Suh, D.; Moon, C. M.; Kim, D.; Baik, S. Ultrahigh Thermal Conductivity of Interface Materials by Silver-Functionalized Carbon Nanotube Phonon Conduits. *Adv. Mater.* **2016**, *28*, 7220−7227.

(9) Yu, A.; Ramesh, P.; Sun, X.; Bekyarova, E.; Itkis, M. E.; Haddon, R. C. Enhanced Thermal Conductivity in a Hybrid Graphite Nanoplatelet—Carbon Nanotube Filler for Epoxy Composites. *Adv. Mater.* **2008**, *20*, 4740−4744.




DOI: 10.1021/acsami.7b12313
*ACS Appl. Mater. Interfaces* 2017, 9, 42067−42074

(10) Huang, X.; Iizuka, T.; Jiang, P.; Ohki, Y.; Tanaka, T. Role of Interface on the Thermal Conductivity of Highly Filled Dielectric Epoxy/AlN Composites. *J. Phys. Chem. C* **2012**, *116*, 13629−13639.
(11) Donnay, M.; Tzavalas, S.; Logakis, E. Boron Nitride Filled Epoxy with Improved Thermal Conductivity and Dielectric Breakdown Strength. *Compos. Sci. Technol.* **2015**, *110*, 152−158.
(12) Hou, G.; Cheng, B.; Ding, F.; Yao, M.; Hu, P.; Yuan, F. Synthesis of Uniform $\alpha$-$Si_3N_4$ Nanospheres by RF Induction Thermal Plasma and Their Application in High Thermal Conductive Nanocomposites. *ACS Appl. Mater. Interfaces* **2015**, *7*, 2873−2881.
(13) Tong, T.; Zhao, Y.; Delzeit, L.; Kashani, A.; Meyyappan, M.; Majumdar, A. Dense Vertically Aligned Multiwalled Carbon Nanotube Arrays as Thermal Interface Materials. *IEEE Trans. Compon. Packag. Technol.* **2007**, *30*, 92−100.
(14) Cola, B. A.; Xu, J.; Fisher, T. S. Contact Mechanics and Thermal Conductance of Carbon Nanotube Array Interfaces. *Int. J. Heat Mass Transfer* **2009**, *52*, 3490−3503.
(15) Wasniewski, J. R.; Altman, D. H.; Hodson, S. L.; Fisher, T. S.; Bulusu, A.; Graham, S.; Cola, B. A. Characterization of Metallically Bonded Carbon Nanotube-based Thermal Interface Materials Using a High Accuracy 1D Steady-State Technique. *J. Electron. Packag.* **2012**, *134*, 020901.
(16) Cross, R.; Cola, B. A.; Fisher, T.; Xu, X.; Gall, K.; Graham, S. A Metallization and Bonding Approach for High Performance Carbon Nanotube Thermal Interface Materials. *Nanotechnology* **2010**, *21*, 445705.
(17) Barako, M. T.; Roy-Panzer, S.; English, T. S.; Kodama, T.; Asheghi, M.; Kenny, T. W.; Goodson, K. E. Thermal Conduction in Vertically Aligned Copper Nanowire Arrays and Composites. *ACS Appl. Mater. Interfaces* **2015**, *7*, 19251−19259.
(18) Xu, J.; Munari, A.; Dalton, E.; Mathewson, A.; Razeeb, K. M. Silver Nanowire Array-Polymer Composite as Thermal Interface Material. *J. Appl. Phys.* **2009**, *106*, 124310.
(19) Chow, J.; Sitaraman, S. K. Electroplated Copper Nanowires as Thermal Interface Materials. *15th IEEE Intersociety Conference on Thermal and Thermomechanical Phenomena in Electronic Systems (ITherm)*, May 31−June 3, 2016; pp 151−155.
(20) Marconnet, A. M.; Panzer, M. A.; Goodson, K. E. Thermal Conduction Phenomena in Carbon Nanotubes and Related Nanostructured Materials. *Rev. Mod. Phys.* **2013**, *85*, 1295−1326.
(21) Prasher, R.; Hu, X. J.; Chalopin, Y.; Mingo, N.; Lofgreen, K.; Volz, S.; Cleri, F.; Keblinski, P. Turning Carbon Nanotubes from Exceptional Heat Conductors into Insulators. *Phys. Rev. Lett.* **2009**, *102*, 105901.
(22) Lian, F.; Llinas, J. P.; Li, Z.; Estrada, D.; Pop, E. Thermal Conductivity of Chirality-Sorted Carbon Nanotube Networks. *Appl. Phys. Lett.* **2016**, *108*, 103101.
(23) Aichlmayr, H. T.; Kulacki, F. A. The Effective Thermal Conductivity of Saturated Porous Media. *Adv. Heat Transfer* **2006**, *39*, 377−460.
(24) ASTM Standard D5470. *Standard Test Method for Thermal Transmission Properties of Thermally Conductive Electrical Insulation Materials*; ASTM International: West Conshohocken, PA, 2012.
(25) Deck, C. P.; Flowers, J.; McKee, G. S. B.; Vecchio, K. Mechanical Behavior of Ultralong Multiwalled Carbon Nanotube Mats. *J. Appl. Phys.* **2007**, *101*, 023512.
(26) Hutchens, S. B.; Needleman, A.; Greer, J. R. Analysis of Uniaxial Compression of Vertically Aligned Carbon Nanotubes. *J. Mech. Phys. Solids* **2011**, *59*, 2227−2237.
(27) Gao, Y.; Kodama, T.; Won, Y.; Dogbe, S.; Pan, L.; Goodson, K. E. Impact of Nanotube Density and Alignment on the Elastic Modulus near the Top and Base Surfaces of Aligned Multi-Walled Carbon Nanotube Films. *Carbon* **2012**, *50*, 3789−3798.
(28) Won, Y.; Gao, Y.; Panzer, M. A.; Dogbe, S.; Pan, L.; Kenny, T. W.; Goodson, K. E. Mechanical Characterization of Aligned Multi-Walled Carbon Nanotube Films Using Microfabricated Resonators. *Carbon* **2012**, *50*, 347−355.
(29) Won, Y.; Gao, Y.; Panzer, M. A.; Xiang, R.; Maruyama, S.; Kenny, T. W.; Cai, W.; Goodson, K. E. Zipping, Entanglement, and the Elastic Modulus of Aligned Single-Walled Carbon Nanotube Films. *Proc. Natl. Acad. Sci. U.S.A.* **2013**, *110*, 20426−20430.
(30) Cao, C.; Reiner, A.; Chung, C.; Chang, S.-H.; Kao, I.; Kukta, R. V.; Korach, C. S. Buckling Initiation and Displacement Dependence in Compression of Vertically Aligned Carbon Nanotube Arrays. *Carbon* **2011**, *49*, 3190−3199.
(31) Maschmann, M. R.; Zhang, Q.; Wheeler, R.; Du, F.; Dai, L.; Baur, J. In Situ Sem Observation of Column-Like and Foam-Like CNT Array Nanoindentation. *ACS Appl. Mater. Interfaces* **2011**, *3*, 648−653.
(32) Ji, L.-W.; Young, S.-J.; Fang, T.-H.; Liu, C.-H. Buckling Characterization of Vertical ZnO Nanowires Using Nanoindentation. *Appl. Phys. Lett.* **2007**, *90*, 033109.
(33) Li, X.; Gao, H.; Murphy, C. J.; Caswell, K. Nanoindentation of Silver Nanowires. *Nano Lett.* **2003**, *3*, 1495−1498.
(34) Bansal, S.; Toimil-Molares, E.; Saxena, A.; Tummala, R. R. Nanoindentation of Single Crystal and Polycrystalline Copper Nanowires. *Proceedings of the 55th Electronic Components and Technology Conference*, 31 May−3 June, 2005; pp 71−76.
(35) Motoyama, M.; Dasgupta, N. P.; Prinz, F. B. Electrochemical Deposition of Metallic Nanowires as a Scanning Probe Tip. *J. Electrochem. Soc.* **2009**, *156*, D431−D438.
(36) Lu, Y.; Peng, C.; Ganesan, Y.; Huang, J. Y.; Lou, J. Quantitative in Situ Tem Tensile Testing of an Individual Nickel Nanowire. *Nanotechnology* **2011**, *22*, 355702.
(37) Motoyama, M.; Prinz, F. B. Electrodeposition and Behavior of Single Metal Nanowire Probes. *ACS Nano* **2014**, *8*, 3556−3566.
(38) Feng, G.; Nix, W. D.; Yoon, Y.; Lee, C. J. A Study of the Mechanical Properties of Nanowires Using Nanoindentation. *J. Appl. Phys.* **2006**, *99*, 074304.
(39) Dou, R.; Derby, B. The Strength of Gold Nanowire Forests. *Scr. Mater.* **2008**, *59*, 151−154.
(40) Starkovich, J. A.; Silverman, E. M.; Tice, J. B.; Peng, H.-H.; Barako, M. T.; Goodson, K. E. High-Conductivity Bonding of Metal Nanowire Arrays. U.S. Patent 9,468,989, 2016.


DOI: 10.1021/acsami.7b12313
*ACS Appl. Mater. Interfaces* 2017, 9, 42067−42074